ACCOUNTS of chemical research

pubs.acs.org/accounts Article

Exotic Topological Bands and Quantum States in Metal–Organic and Covalent–Organic Frameworks

Wei Jiang,[§] Xiaojuan Ni,[§] and Feng Liu*

Cite This: *Acc. Chem. Res.* 2021, 54, 416–426 Read Online

ACCESS | Metrics & More | Article Recommendations

CONSPECTUS: Metal–organic and covalent–organic frameworks (MOFs/COFs) have been extensively studied for fundamental interests and their promising applications, taking advantage of their unique structural properties, i.e., high porosity and large surface-to-volume ratio. However, their electronic and magnetic properties have been somewhat overlooked because of their relatively poor performance as conductive and/or magnetic materials. Recent experimental breakthroughs in synthesizing two-dimensional (2D) π-conjugated MOFs/COFs with high conductivity and robust magnetism through doping have generated renewed and increasing interest in their electronic properties. Meanwhile, comprehensive theoretical studies of the underlying physical principles have led to discovery of many exotic quantum states, such as topological insulating states, which were only observed in inorganic systems. Especially, the diversity and high tunability of MOFs/COFs have provided a playground to explore novel quantum physics and quantum chemistry as well as promising applications.

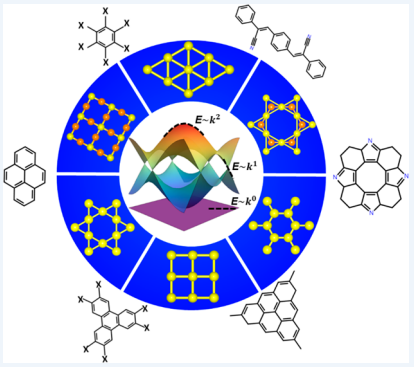

The band theory has empowered us to understand the most fundamental electronic properties of inorganic crystalline materials, which can also be used to better understand MOFs/COFs. The first obvious difference between the two is that instead of atomic orbitals residing at lattice sites of inorganic crystals, molecular orbitals of organic ligands are predominant in MOFs/COFs. The second key difference is that usually all atomic orbitals in an inorganic crystal are subject to one common group of lattice symmetry, while atomic orbitals of metal ion and molecular orbitals of different organic ligands in MOFs/COFs belong to different subgroups of lattice symmetries. Both these differences will impact the band structure of MOFs/COFs, in particular making it more complex. Consequently, which subset of bands are of most importance depends strongly on the location of Fermi level, i.e., electron counting and charge doping. Furthermore, there are usually two types of characteristic electrons coupled in MOFs, i.e., strongly correlated localized *d* and *f* electrons and diffusive *s* and *p* electrons, which interplay with lattice, orbital, and spin degrees of freedom, leading to more exotic topological and magnetic band structures.

In this Account, we present an up-to-date review of recent theoretical developments to better understand the exotic band structures of MOFs/COFs. Starting from three fundamental 2D lattice models, i.e., honeycomb, Kagome, and Lieb lattices, exotic Dirac and flat bands as well as the intriguing topological quantum states they host, e.g., quantum spin Hall and quantum anomalous Hall states, are outlined. In addition to the single-lattice models, we further elaborate on combined lattice model Hamiltonians, which give rise to overlapping bands hosting novel quantum states, such as nodal-line Dirac semimetal and unconventional superconducting states. Also, first-principles predictions of candidate MOFs/COFs that host these exotic bands and hence quantum phases are reviewed, which greatly extends the pool of materials beyond inorganic crystals for hosting exotic band structures.

KEY REFERENCES

- Wang, Z. F.; Liu, Z.; Liu, F. Organic Topological Insulators in Organometallic Lattices. *Nat. Commun.* **2013**, *4*, 1471.[1] *This is the pioneering theoretical work predicting the quantum spin Hall effect in 2D MOFs.*
- Liu, Z.; Wang, Z. F.; Mei, J. W.; Wu, Y. S.; Liu, F. Flat Chern Band in a Two-Dimensional Organometallic Framework. *Phys. Rev. Lett.* **2013**, *110*, 106804.[2] *This is the first theoretical study of a flat Chern band in MOFs.*
- Wang, Z. F.; Su, N.; Liu, F. Prediction of a Two-Dimensional Organic Topological Insulator. *Nano Lett.*, **2013**, *13* 2842–2845.[3] *This is the first theoretical work reporting a 2D topological insulator and quantum spin Hall effect in experimentally synthesized MOFs.*
- Jiang, W.; Huang, H.; Liu, F. A Lieb-like Lattice in a Covalent-Organic Framework and Its Stoner Ferromagnetism. *Nat. Commun.* **2019**, *10*, 2207.[4] *This is the first*

Received: October 5, 2020
Published: January 5, 2021

https://dx.doi.org/10.1021/acs.accounts.0c00652
Acc. Chem. Res. 2021, 54, 416–426

theoretical report of Lieb lattice realization in COFs and its Stoner ferromagnetism.

INTRODUCTION

Electronic band structure essentially describes the relationship between electron energy and wavevector, i.e., momentum, called the dispersion relation. For a free electron in vacuum, its wave function takes the form of a plane wave $\varphi(\vec{r},t) = A\, e^{i(\vec{k}\vec{r}-\omega t)}$, which naturally leads to a parabolic dispersion $E(k) \propto k^2$. For an electron in crystals, its wave function is modulated by the periodic crystal potential into the Bloch wave function $\psi(\vec{r},t) = \varphi(\vec{r},t)\, u(\vec{r})$, where u is a periodic function of crystal lattice. In materials with a weak crystal field of level splitting, such as in metals, electrons are nearly free with a continuous energy spectrum (band); while in those with a strong crystal field, such as in semiconductors and insulators, electrons become localized, having a gapped energy spectrum with certain range of forbidden energies (band gap). Different from free electrons with a constant rest mass (m_0), electrons in crystals behave like quasi-particles, whose low-energy excitations depend on electron−ion and electron−electron interactions, manifesting in different band dispersions and effective masses (m^*). In general, the band dispersion in almost all crystals keeps the "normal" parabolic function, i.e., $E(k) \propto k^2$, albeit with a different coefficient, i.e., effective mass (Figure 1a).

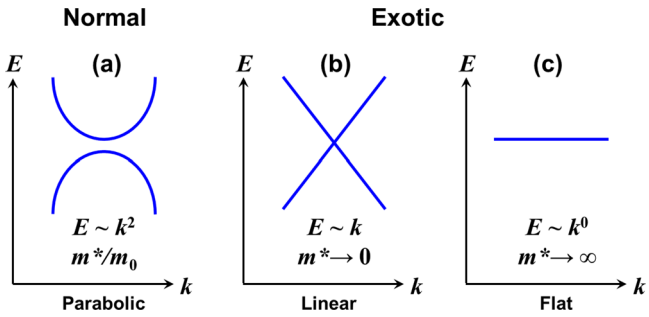

Figure 1. Illustrations of band structures. (a) Usual parabolic bands with a finite electron effective mass. Exotic bands: (b) linear Dirac bands with a zero effective mass and (c) flat band with an infinite effective mass.

It is noted that considering the special relativity effect, the dispersion relation of a free electron in vacuum becomes linear, $E(k) \propto k$ (Figure 1b), i.e., the solution of the Dirac equation instead of the Schrödinger equation. Surprisingly, an analog of such "exotic" linear band dispersion (Dirac band) was discovered in 2005 in graphene,[5] a two-dimensional (2D) crystal with a honeycomb lattice, although the theoretical calculation of its Dirac band was already conducted early in 1947.[6] Also, it has been theoretically shown that even a completely nondispersive flat band,[7] i.e., $E(k) \propto k^0$ (Figure 1c), may arise in certain lattices with special symmetry, such as 2D Kagome and Lieb lattices.[8−11] The topological flat band is formed by phase cancellation of Bloch wave functions, i.e., destructive quantum interference[7] leading to compact localized states characterized with canceling outward lattice hopping, as illustrated in Figure 2, which is distinctively different from the trivial flat band, formed by localized dangling bond without hopping.[12] Such exotic band structures endow electrons with unusual properties, especially novel quantum states. The linear-dispersive Dirac bands have massless electrons like a photon

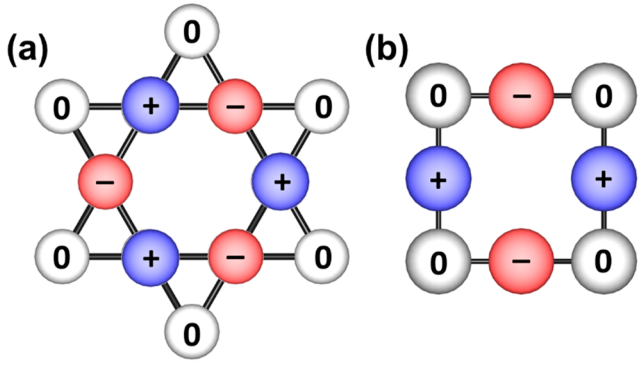

Figure 2. Localized eigenstate of the flat band in real space of a (a) Kagome lattice and (b) Lieb lattice. The blue and red colors indicate the positive and negative phase of the nodes of wave function at lattice sites.

(Figure 1b), while the nondispersive flat bands host electrons with an infinite mass (Figure 1c). The completely quenched electron kinetic energy in a flat band renders naturally a strongly interactive and correlated quantum system, because any small finite interaction energy is still much larger than "zero" kinetic energy.

Furthermore, both Dirac and flat bands have inherently a so-called nontrivial band topology.[13] The mathematical concept of topology is used to classify different manifolds that cannot be "continuously deformed" into each other. Similarly, band topology is introduced to classify different band structures that cannot be "adiabatically connected" with each other.[14] One may imagine when atoms were brought together to form solids, atomic levels would spread to form bands. In general, an insulating solid is a normal insulator of trivial band topology if it can be adiabatically connected (without gap closure or band inversion) to the "atomic limit"; otherwise, it is a topological insulator (TI) characterized with a spin−orbit coupling (SOC) gap.[14] If the degeneracy of the band crossing point, e.g., the Dirac point, is protected by some crystalline symmetries in the presence of SOC, then the solid is a topological semimetal. The band topology can be identified by calculating its topological invariant, and a nonzero invariant means that as the phase of electron Bloch wave function (Berry phase)[15] evolves in the parameter space of momenta, it changes integer times of π. This translates into a quantized and spin selective Hall conductivity, in analogy to the quantum Hall effect where the external magnetic field imposes a topological phase evolution of the wave function of 2D free electron gas, where the mathematical concept of topology was first used in the context of physics condensed matter.[16] For this reason, topological materials, i.e., materials with nontrivial band topology like Dirac and flat bands, hold promising applications in quantum information and computing as well as spintronics devices.

The discovery of graphene has fostered an ever-growing field of 2D materials, including 2D topological and quantum materials.[17,18] In this Account, we will focus on reviewing recent studies of 2D organic topological and quantum materials, in particular MOFs/COFs featured with topological Dirac and flat bands, which are sometimes called Dirac and flat-band materials.[19−21] The readers are referred to some recent review articles on related topics, in particular inorganic quantum materials, for more information.[22,23] The Dirac and flat bands generally arise in 2D lattices having special lattice and orbital symmetries that warrant some desirable phase cancellation of Bloch wave functions. The Dirac band in graphene is derived

https://dx.doi.org/10.1021/acs.accounts.0c00652
Acc. Chem. Res. 2021, 54, 416−426

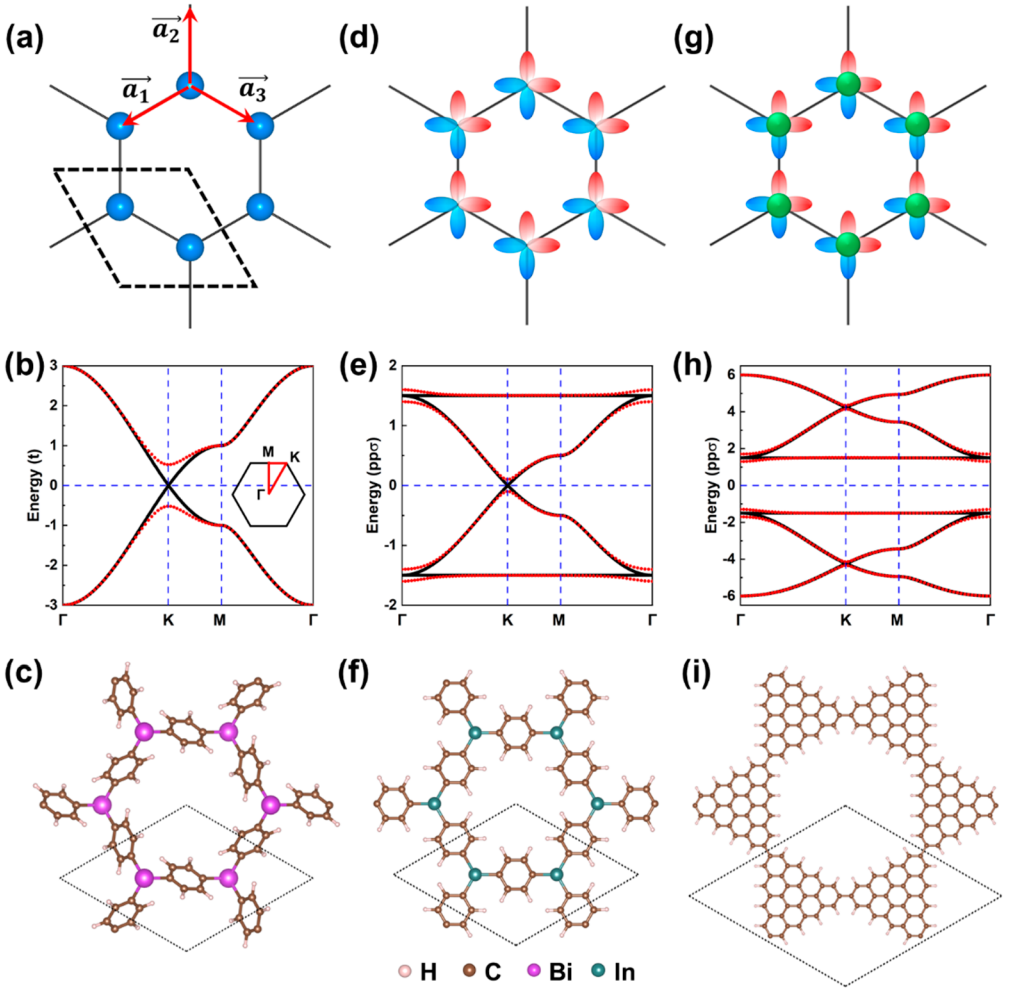

Figure 3. Illustrations of a honeycomb lattice consisting of (a) single orbital, (d) (p_x, p_y) orbitals, and (g) (s, p_x, p_y) orbitals on each lattice site. (b) The Dirac bands without (black) and with (red) SOC of (a) with $\varepsilon = 0$ and $\lambda = 0.2t/\sqrt{3}$. The inset in (b) shows the first Brillouin zone of a honeycomb lattice. (c) Representative MOF hosting Dirac bands.[1] (e) Four bands without (black) and with (red) SOC of (d) with $\varepsilon = 0$, $pp\pi = 0$, and $\lambda = 0.1pp\sigma$. (f) Representative MOF hosting four bands.[2] (h) Enantiomorphic Kagome bands without (black) and with (red) SOC of (c) with $\varepsilon = 0$, $ss\sigma = -2pp\sigma$, $sp\sigma = 2pp\sigma$, $pp\pi = 0$, and $\lambda = 0.2pp\sigma$. (i) Representative COF hosting enantiomorphic Kagome bands. The dashed rhombus indicates the unit cell in (a), (c), (f), and (i).

from inversion symmetry between two sub trigonal lattices and C_3 rotational symmetry; the flat band usually forms in a geometrically frustrated lattice, such as Kagome (corner-shared triangle) and Lieb (edge-centered square) lattices,[8,9] where complete phase cancellation of lattice wave functions is warranted. There is a very large family of 2D MOFs/COFs, and many of them may satisfy such symmetry requirements, especially considering the extraordinary diversity of coordination chemistry that will provide countless combinations of metal ions and organic linkers, to offer a rich variety of lattice, orbital, and spin symmetries.[24,25] This makes MOFs/COFs an ideal material platform to realize the exotic Dirac and flat bands.

In the following, we will start with introducing a generic tight-binding (TB) model in three basic 2D lattices, i.e., honeycomb, Kagome, and Lieb lattices, with single/multiple orbital hopping, to demonstrate the formation mechanisms of Dirac and flat bands as well as their associated intriguing quantum states, e.g., quantum spin Hall (QSH)[17] and quantum anomalous Hall (QAH)[26] states, and flat-band ferromagnetism induced by high density of state and enhanced correlation effect when the flat band is partially filled.[8] We also discuss briefly the combined honeycomb and Kagome lattice model and resulting quantum states. Furthermore, original first-principles calculations that have predicted the selected MOFs/COFs hosting the Dirac and/or flat bands will be reviewed with the features of their quantum states analyzed. Lastly, we discuss the experimental challenges in synthesizing large-sample size of crystalline MOFs/COFs and further characterizing their topological properties.

TIGHT-BINDING MODEL

The Hamiltonian of a generic TB model with single-orbital (s or p_z) or multiorbital [(p_x, p_y) or (s, p_x, p_y)] hopping in a lattice can be expressed as

https://dx.doi.org/10.1021/acs.accounts.0c00652
Acc. Chem. Res. 2021, 54, 416−426

$$H = \sum_{i\alpha} \varepsilon_{i\alpha} c_{i\alpha}^{\dagger} c_{i\alpha} - \left(\sum_{\langle i\alpha, j\beta \rangle} t c_{i\alpha}^{\dagger} c_{j\beta} + \sum_{\langle\langle i\alpha, j\beta \rangle\rangle} t_2 c_{i\alpha}^{\dagger} c_{j\beta} + \sum_{\langle\langle\langle i\alpha, j\beta \rangle\rangle\rangle} t_3 c_{i\alpha}^{\dagger} c_{j\beta} \right) + i\lambda \sum_{\langle\langle i\alpha, j\beta \rangle\rangle} c_{i\alpha}^{\dagger} \sigma_z \left(\frac{\vec{d}_{jk}}{|\vec{d}_{jk}|} \times \frac{\vec{d}_{ki}}{|\vec{d}_{ki}|} \right) c_{j\beta} + M \sum_{i\alpha} c_{i\alpha}^{+} \sigma_z c_{i\alpha} \quad (1)$$

where $\varepsilon_{i\alpha}$ is the on-site energy of the α orbital at the ith site. $c_{i\alpha}^{\dagger} = (c_{i\alpha\uparrow}^{\dagger}, c_{i\alpha\downarrow}^{\dagger})$ and $c_{i\alpha} = (c_{i\alpha\uparrow}, c_{i\alpha\downarrow})$ are electron creation and annihilation operators of the α orbital at the ith site, respectively. $\langle\langle i,j \rangle\rangle$, $\langle\langle i,j \rangle\rangle$, and $\langle\langle\langle i,j \rangle\rangle\rangle$ denote the nearest-neighbor (NN), second NN (2NN), and third NN (3NN) hopping with hopping parameters t, t_2, and t_3, respectively, which are expressed within the Slater−Koster scheme.[27] The third term is the 2NN intrinsic SOC with magnitude λ. σ_z is the z-component of Pauli matrix, and $\vec{d}_{ki}$ is the vector from site i to site k. The last term is the exchange field with magnitude M. For the lattice model with (p_x, p_y)- or (s, p_x, p_y)-orbital hopping, the third term will be replaced with the on-site SOC expressed as $\lambda \hat{L} \cdot \hat{\sigma}$, where $\hat{L}$ is the angular momentum operator and $\hat{\sigma}$ are the Pauli matrices. By transforming the Hamiltonian (eq 1) into momentum space, one obtains the k-space Hamiltonian $H(\vec{k}) = \begin{pmatrix} \varepsilon & H_0 \\ H_0^* & \varepsilon \end{pmatrix}$. The TB model is equivalent to the extended Hückel model adopting periodic boundary condition, with a proper transformation of lattice hopping parameters between the two models. Later we will discuss the exact expressions of ε and H_0 for each lattice type.

To characterize band topology, for system with inversion symmetry without exchange field, the topological invariant Z_2 number[28] can be derived based on the parity at time-reversal invariant momenta that classifies topologically trivial ($Z_2 = 0$) or nontrivial ($Z_2 = 1$) states.[29] The nontrivial system represents a 2D TI exhibiting the QSH effect, characterized with two helical edge states of quantized spin Hall conductivity. For system with broken time reversal symmetry, where the exchange field separates two spin channels with only one spin component at the Fermi level, the Chern number is used to characterize the topology, which is defined as[30]

$$C = \frac{1}{2\pi} \int_{BZ} d^2k F_{12}(k) \quad (2)$$

where $F_{12}(k) = \frac{\partial}{\partial k_1} A_2(k) - \frac{\partial}{\partial k_2} A_1(k)$ is the Berry curvature, $A_\mu(k) = -i \left\langle n_k \left| \frac{\partial}{\partial k_\mu} \right| n_k \right\rangle$ is the Berry connection, and $|n_k\rangle$ is a normalized wave function of the respective band. The nontrivial system of nonzero Chern number represents a Chern insulator (CI) exhibiting the QAH effect, characterized with the Chern numbers of chiral edge states with quantized charge and spin Hall conductivity. For TIs, the Chern number may be calculated for each spin component of bands ($C_\uparrow$ and $C_\downarrow$), and the spin Chern number, $C_s = \frac{1}{2}(C_\uparrow - C_\downarrow)$, may be used loosely in equivalence with the Z_2 number.

HONEYCOMB LATTICE

The model of single-orbital hopping in a honeycomb lattice is shown in Figure 3a. Its k-space Hamiltonian is

$$H(\vec{k}) = \begin{pmatrix} \varepsilon_0 & -t(e^{ik_1} + e^{ik_2} + e^{ik_3}) \\ -t(e^{-ik_1} + e^{-ik_2} + e^{-ik_3}) & \varepsilon_0 \end{pmatrix} \quad (3)$$

where k_n is defined as $k_n = \vec{k} \cdot \vec{a}_n$ with three NN hopping vectors $\vec{a}_1 = \left(-\frac{\sqrt{3}}{2}\hat{x} - \frac{1}{2}\hat{y} \right), \vec{a}_2 = \hat{y}$, and $\vec{a}_3 = \left(\frac{\sqrt{3}}{2}\hat{x} - \frac{1}{2}\hat{y} \right)$, labeled in Figure 3a, which is also adopted in the following discussions. As originally developed for graphene, this simple model gives rise to two Dirac bands, as shown in Figure 3b. Further inclusion of SOC opens a nontrivial gap at the Dirac points, $K(K')$, changing the system from a topological semimetal into a TI.[17] The two Dirac bands have opposite spin Chern numbers. The first organic TI (OTI) with Dirac bands in a honeycomb lattice was theoretically predicted by Wang et al., in the MOF of $Bi_2(C_6H_4)_3$ and $Pb_2(C_6H_4)_3$.[1] The Bi ions are located at the honeycomb lattice sites (Figure 3c), which give rise to the Dirac bands and a SOC gap of 43 meV at the Dirac point. The nontrivial topology of $Bi_2(C_6H_4)_3$ has been theoretically confirmed by the edge states and nonzero Z_2 number. However, the topological gap in $Bi_2(C_6H_4)_3$ is not intrinsic, because it is not aligned with the Fermi level. Electron doping is needed to move the Fermi level into the gap. This original work has since stimulated a number of subsequent theoretical predictions of OTIs, such as replacing the metal ions with Pd,[1] In,[2] Tl,[31] Mn,[32,33] Fe,[33] and V.[33] We note that there was a later theoretical study of $Pb_2(C_6H_4)_3$ MOF showing an antiferromagnetic ground state and topological phases;[34] the difference is likely due to different functional used in the calculation. Recently, a COF formed by triangulenes[35] has been experimentally synthesized[36] and theoretically predicted to be Dirac semimetal.[37,38]

Besides the single-orbital honeycomb model, there can be multiple orbitals on each lattice site, such as two (p_x, p_y)-orbitals, as illustrated in Figure 3d. The matrix elements ε and H_0 of the Hamiltonian are expressed as

$$\varepsilon = \begin{pmatrix} \varepsilon_{p_x} & 0 \\ 0 & \varepsilon_{p_y} \end{pmatrix} \text{ and}$$

$$H_0 = -\begin{pmatrix} \frac{1}{4}(3pp\sigma + pp\pi)(e^{ik_1} + e^{ik_3}) + pp\pi\, e^{ik_2} & \frac{\sqrt{3}}{4}(pp\sigma - pp\pi)(e^{ik_1} - e^{ik_3}) \\ \frac{\sqrt{3}}{4}(pp\sigma - pp\pi)(e^{ik_1} - e^{ik_3}) & \frac{1}{4}(pp\sigma + 3pp\pi)(e^{ik_1} + e^{ik_3}) + pp\sigma\, e^{ik_2} \end{pmatrix} \quad (4)$$

Assuming a vanishing $pp\pi$ (usually much smaller than $pp\sigma$), this TB model gives four bands consisting of two Dirac bands sandwiched by two flat bands (Figure 3e). The Dirac points at $K(K')$ and two band touching points at Γ will be gapped by SOC. All three gaps are topologically nontrivial, as characterized by their band-resolved spin Chern numbers from top to bottom: 1, 0, 0, −1.[39−41] This TB model has been realized theoretically first in MOFs of $In_2(C_6H_4)_3$ (Figure 3f)[2] and then $Tl_2(C_6H_4)_3$,[31] in which the four bands near the Fermi level are predominantly contributed by p_x and p_y orbitals of metal ions. When the flat band is partially filled, it is subjected to a spin polarization due to its strong Coulomb repulsion, and the fractional Chern insulator state could be achieved.[2]

Another intriguing system with multiorbitals per site in a honeycomb lattice is the (s, p_x, p_y)-orbital hopping model, as

https://dx.doi.org/10.1021/acs.accounts.0c00652
Acc. Chem. Res. 2021, 54, 416−426

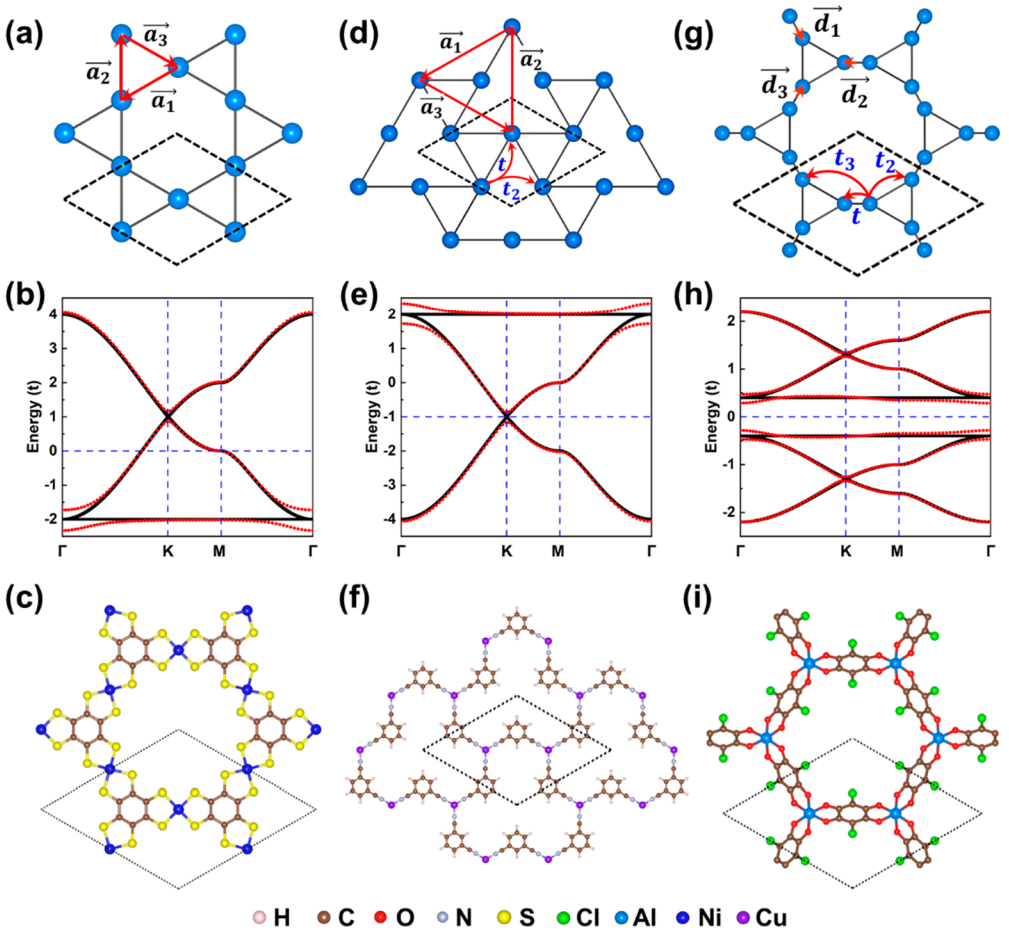

Figure 4. Illustrations of lattice models consisting of single orbital in (a) Kagome, (d) coloring-triangle (CT), and (g) diatomic Kagome lattices. (b) Kagome bands without (black) and with (red) SOC of (a) with $\varepsilon = 0$ and $\lambda = 0.3t$. (c) Representative MOF hosting Kagome lattice bands.[3] (e) Kagome bands without (black) and with (red) SOC of (b) with $\varepsilon = 0$, $t_2 = 0$, and $\lambda = 0.3t$. (f) Representative MOF hosting Kagome bands of a CT lattice.[44] (h) Enantiomorphic Kagome bands without (black) and with (red) SOC of (c) with $\varepsilon = 0$, $t_2 = 0$, $t_3 = 0.3t$, and $\lambda = 6t/\sqrt{3}$. (i) Representative MOF hosting enantiomorphic Kagome bands.[45] The first Brillouin Zone of a Kagome lattice is the same as that of a honeycomb lattice, as represented by the inset of Figure 1b. The dashed rhombus indicates the unit cell in (a), (c), (d), (f), (g), and (i).

illustrated in Figure 3g. The corresponding ε and H_0 are expressed as

$$\varepsilon = \begin{pmatrix} \varepsilon_s & 0 & 0 \\ 0 & \varepsilon_{p_x} & 0 \\ 0 & 0 & \varepsilon_{p_y} \end{pmatrix} \text{ and}$$

$$H_0 = -\begin{pmatrix} ss\sigma(e^{ik_1} + e^{ik_2} + e^{ik_3}) & -\frac{\sqrt{3}}{2}sp\sigma(e^{ik_1} - e^{ik_3}) & -\frac{1}{2}sp\sigma(e^{ik_1} - 2e^{ik_2} + e^{ik_3}) \\ \frac{\sqrt{3}}{2}sp\sigma(e^{ik_1} - e^{ik_3}) & \frac{1}{4}(3pp\sigma + pp\pi)(e^{ik_1} + e^{ik_3}) + pp\pi e^{ik_2} & \frac{\sqrt{3}}{4}(pp\sigma - pp\pi)(e^{ik_1} - e^{ik_3}) \\ \frac{1}{2}sp\sigma(e^{ik_1} - 2e^{ik_2} + e^{ik_3}) & \frac{\sqrt{3}}{4}(pp\sigma - pp\pi)(e^{ik_1} - e^{ik_3}) & \frac{1}{4}(pp\sigma + 3pp\pi)(e^{ik_1} + e^{ik_3}) + pp\sigma e^{ik_2} \end{pmatrix} \quad (5)$$

By simply setting $pp\pi = 0$, one obtains the enantiomorphic Yin−Yang Kagome bands,[42] as shown in Figure 3h. With SOC, the band-resolved spin Chern numbers from top to bottom are 1, 0, −1, 1, 0, −1. It is worth noting that the spin Chern numbers of the two sets of Kagome bands are opposite of each other (named as Yin−Yang Kagome bands)[42] and especially the two flat bands separated by the Fermi level have opposite signs, which spawns various intriguing excited-state quantum phenomena, such as the excited quantum Hall effect and giant circular dichroism.[42,43] The COF formed by graphene nanoflakes (Figure 3i) may host such a band structure based on the (s, p_x, p_y)-orbital honeycomb model. The molecular orbitals (MOs)

https://dx.doi.org/10.1021/acs.accounts.0c00652
Acc. Chem. Res. 2021, 54, 416−426

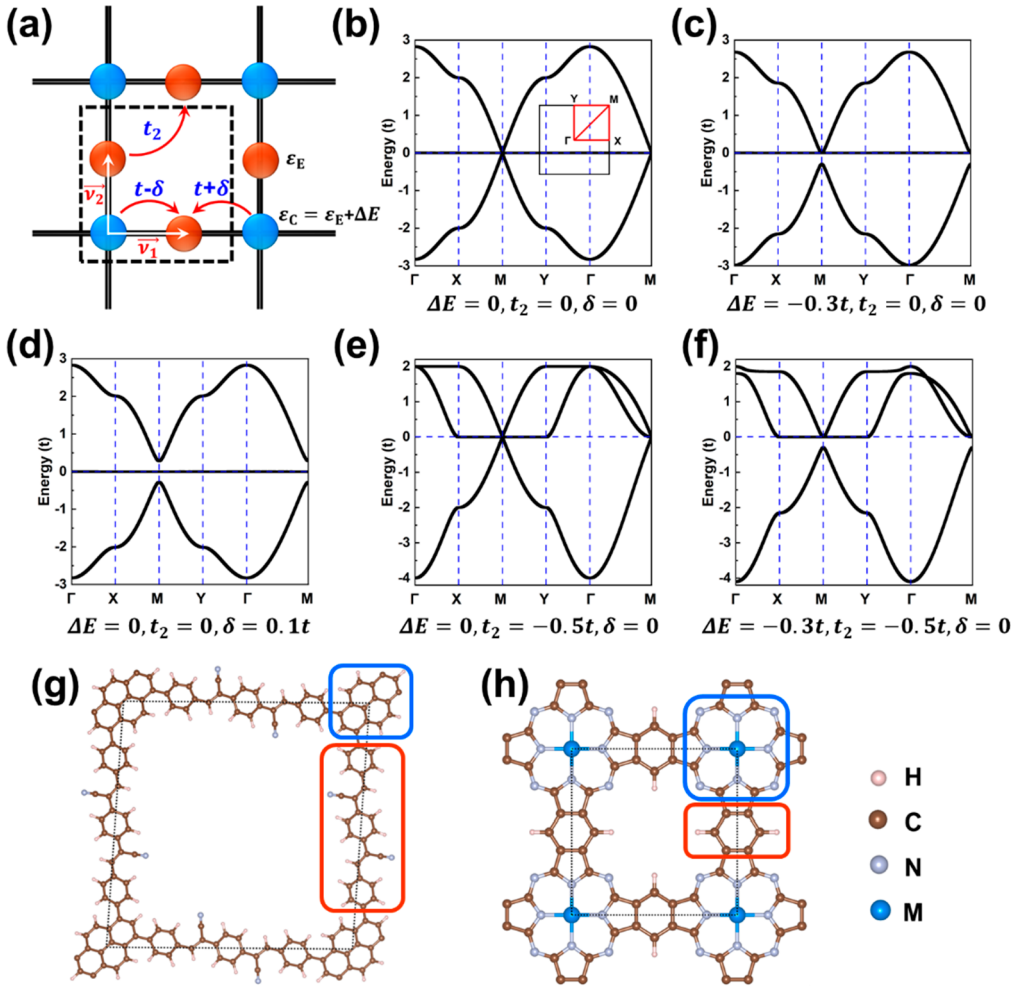

Figure 5. Band structure evolution in Lieb lattices. (a) Lieb lattice structure with one corner and two edge-center states. t, t_2, δ, and ΔE denote NN hopping, 2NN hopping, dimerization term, and on-site energy difference, respectively. (b–f) Band structures of the Lieb lattice with their corresponding parameters indicated with each plot. (g) COF with a strained Lieb lattice, sp^2-COF Py(BCSB)$_2$, whose corner and edge-center sites are made of Py (orange rectangle) and BCSB (blue) ligand, respectively. (h) Same as (g) for MPc-MOF, with Pc and benzene molecules make up the corner and edge-center sites, respectively.

of the organic ligand near the Fermi level have the same shape and symmetry as the atomic s, p_x, and, p_y orbitals, which serve effectively as the "super-atomic" orbital basis to form the enantiomorphic Yin-Yang Kagome bands.

KAGOME AND RELATED LATTICES

The single-orbital hopping in a Kagome lattice is shown in Figure 4a. Its k-space Hamiltonian is

$$H(\vec{k}) = \begin{pmatrix} \varepsilon_0 & -2t\cos k_3 & -2t\cos k_2 \\ -2t\cos k_3 & \varepsilon_0 & -2t\cos k_1 \\ -2t\cos k_2 & -2t\cos k_1 & \varepsilon_0 \end{pmatrix} \quad (6)$$

which yields three bands with one flat band located either below or above two Dirac bands depending on the sign (positive vs negative) of lattice hopping (Figure 4b). Similarly, after considering SOC effect, the Dirac points at $K(K')$ and band touching point at Γ will be gapped, leading to TI states. For both spins, the flat band and bottom Dirac band have a nonzero spin Chern number of opposite sign and the middle Dirac band has a zero spin Chern number.

The realization of Kagome bands in MOFs/COFs has been extensively studied since 2013. The pioneering work is the theoretical prediction of QSH effect in $Ni_3(C_6S_6)_2$,[3] which consists of three Ni ions being located at Kagome sites, as shown in Figure 4(c). It is noted that based on a bottom-up gas–liquid interfacial reaction approach, a monolayer of $Ni_3(C_6S_6)_2$ has been synthesized in the same year.[46] $Ni_3(C_6S_6)_2$ was shown to have one flat band above two Dirac bands near the Fermi level; its nontrivial topology were demonstrated with topological edge states and quantized spin Hall conductivity.[3] Based on the same design principle demonstrated in $Ni_3(C_6S_6)_2$, several other MOFs[47−49] have been subsequently proposed to possess the topological Kagome bands, which greatly enriches the materials platform for experimental confirmation. An experiment work has indicated the existence of flat band in a ferromagnetic MOF Kagome lattice of Cu(1,3-bdc) and suggested possible topological magnon state.[50]

Interestingly, another lattice, called coloring-triangle (CT) lattice (Figure 4d), has been shown to have the identical Kagome bands as that of a Kagome lattice, as the two lattice Hamiltonians can converted into each other via a unitary transformation.[51] The k-space Hamiltonian of the CT lattice is

https://dx.doi.org/10.1021/acs.accounts.0c00652
Acc. Chem. Res. 2021, 54, 416−426

$$H(\vec{k}) = \begin{pmatrix} \varepsilon_0 & -t(e^{ik_1-k_2/3} + e^{ik_3-k_1/3}) & -t(e^{ik_3-k_2/3} + e^{ik_1-k_3/3}) \\ -t(e^{ik_2-k_1/3} + e^{ik_1-k_3/3}) & \varepsilon_0 & -t(e^{ik_2-k_3/3} + e^{ik_1-k_2/3}) \\ -t(e^{ik_2-k_3/3} + e^{ik_3-k_1/3}) & -t(e^{ik_3-k_2/3} + e^{ik_2-k_1/3}) & \varepsilon_0 \end{pmatrix} \quad (7)$$

The NN hopping of intratriangle and intertriangle in the CT lattice are indicated by t and t_2[see Figure 4(d)]. By introducing a 2D periodic potential to physically make t_2 vanishing, the CT lattice can host perfect Kagome bands, as shown in Figure 4(e). The MOF of $Cu_2(C_8N_2H_4)_3$ [Figure 3(f)] with a geometry of CT lattice has been shown to be a QAH insulator.[44] Its electronic band structure and topological properties can be well explained by the physics of Kagome bands of the CT lattice.

Another type of Kagome lattice is the diatomic Kagome lattice consisting of two atoms sitting on each Kagome lattice site, as shown in Figure 4g. The corresponding ε and H_0 are

$$\varepsilon = \begin{pmatrix} \varepsilon_0 & 0 & 0 \\ 0 & \varepsilon_0 & 0 \\ 0 & 0 & \varepsilon_0 \end{pmatrix} \text{ and}$$

$$H_0 = -\begin{pmatrix} t\, e^{-i\vec{k}\cdot 2\vec{d}_1} & t_3 \cos k_3\, e^{i\vec{k}\cdot\vec{d}_3} & t_3 \cos k_2\, e^{i\vec{k}\cdot\vec{d}_2} \\ t_3 \cos k_3\, e^{i\vec{k}\cdot\vec{d}_3} & t\, e^{-i\vec{k}\cdot 2\vec{d}_2} & t_3 \cos k_1\, e^{i\vec{k}\cdot\vec{d}_1} \\ t_3 \cos k_2\, e^{i\vec{k}\cdot\vec{d}_2} & t_3 \cos k_1\, e^{i\vec{k}\cdot\vec{d}_1} & t\, e^{-i\vec{k}\cdot 2\vec{d}_3} \end{pmatrix} \quad (8)$$

respectively, where $\vec{d}_1 = d\left(\frac{\vec{a}_3 - \vec{a}_2}{|\vec{a}_3 - \vec{a}_2|}\right)$, $\vec{d}_2 = d\left(\frac{\vec{a}_1 - \vec{a}_3}{|\vec{a}_1 - \vec{a}_3|}\right)$, and $\vec{d}_3 = d\left(\frac{\vec{a}_2 - \vec{a}_1}{|\vec{a}_2 - \vec{a}_1|}\right)$. Here, d is the displacement of the two dumbbell atoms away from the Kagome site, as indicated in Figure 4g. For simplicity, one can neglect t_2, which will not affect the band structure qualitatively in a wide range of parameter space.[42] The TB band structure is shown in Figure 4h, consisting of a pair of enantiomorphic Kagome bands. With SOC, the two flat bands have the opposite sign of spin Chern numbers, originating from the same physics as described above by the TB model of (s, p_x, p_y)-orbital hopping in a honeycomb lattice.

To realize the Yin−Yang Kagome bands in a diatomic Kagome lattice, the longer-distance cross hopping between two sub-Kagome lattices needs to be larger than the shorter-distance interatomic hopping. This intriguing lattice hopping condition makes the suitable diatomic-Kagome lattice materials rather limited. It is noted that in a Kagome lattice with a dual of frontier π-orbitals per lattice site, the Yin-Yang Kagome bands have been disclosed in an anilato-based MOF $Al_2(C_6O_4Cl_2)_3$ [Figure 4(i)].[45] The topological property of $Al_2(C_6O_4Cl_2)_3$ has been theoretically demonstrated by the presence of topological edge states and nonzero Z_2 number. The anilato-based MOFs not only significantly expands the pool of materials hosting enantiomorphic Yin-Yang Kagome bands, but also provides a new platform to study π-orbital originated quantum chemistry and physics.

LIEB LATTICE

In addition to the Kagome lattice, another 2D lattice that hosts both Dirac and flat bands is the Lieb lattice, i.e., the edge-centered square lattice (Figure 5a). The band topology of the two lattices is closely related because they are both line-graph lattices and interconvertible via strain.[52] Although with different lattice symmetries, the two can be viewed sharing the same structural configuration, i.e., one corner site and two edge-center sites. Different from the Kagome lattice that has been realized in many real material systems, materials that host Lieb band structure are quite rare, mainly because the flat band can only survive in an ideal Lieb lattice with the same on-site energies for the corner and edge-center sites of different bonding environment and negligible 2NN lattice hopping. This can be understood by inspecting closely its k-space Hamiltonian,

$$H(\vec{k}) = \begin{pmatrix} \varepsilon_C & -2t\cos(\vec{k}\cdot\vec{v}_1) & -2t\cos(\vec{k}\cdot\vec{v}_2) \\ -2t\cos(\vec{k}\cdot\vec{v}_1) & \varepsilon_E & -4t_2\cos(\vec{k}\cdot\vec{v}_1)(\vec{k}\cdot\vec{v}_2) \\ -2t\cos(\vec{k}\cdot\vec{v}_2) & -4t_2\cos(\vec{k}\cdot\vec{v}_1)(\vec{k}\cdot\vec{v}_2) & \varepsilon_E \end{pmatrix} \quad (9)$$

where $\vec{v}_1 = \hat{x}$ and $\vec{v}_2 = \hat{y}$, respectively. It generally should have two different on-site energies (ε_E and $\varepsilon_C = \varepsilon_E + \Delta E$) for the edge-center and corner site, respectively, and two different lattice hoppings (the NN hooping t between the corner and edge-center sites vs the 2NN hopping t_2 between the edge-center sites), according to its D_{4h} symmetry. Ideal Lieb band structure with one perfect flat band crossing the middle of Dirac bands (Figure 5b) arises only if $\varepsilon_E = \varepsilon_C$ and $t_2 = 0$, which is unlikely, if not impossible, to be the case in real materials. Nonzero ΔE leads to an energy gap opening at the M point either below or above the flat band, depending on the sign of ΔE (Figure 5c for negative ΔE), and nonzero t_2 induces band dispersion in the middle flat band (Figure 5e). When a dimerization interaction: $t \rightarrow t \pm \delta$ is present, two gaps open below and above the flat band (Figure 5d). Both ΔE and δ represent certain degrees of electron inhomogeneity in the system. Because of the nonvanishing ΔE, δ, and t_2, real materials can only fulfill a nonideal Lieb lattice, whose band structure is always distorted or disguised (Figure 5f). For this reason, a Lieb band structure and hence a Lieb lattice can be easily overlooked.

The first Lieb lattice material has been recently demonstrated in an sp^2 carbon-conjugated COF (sp^2-COF),[4,53] which was experimentally discovered to host stable ferromagnetism upon hole doping.[54] The molecular structure is shown in Figure 5g, which can be viewed as an assembly of pyrene (Py) and 1,4-bis(cyanostyryl)benzene (BCSB) ligands that occupy the corner (blue ellipse) and edge-center sites (red ellipse), respectively, of a Lieb lattice which is slightly strained along the diagonal direction. The Lieb nature of the sp^2-COF lattice, $Py(BCSB)_2$, is revealed by analyzing the molecular orbitals of the two building units, i.e., Py and BCSB, and the corresponding orbital-resolved bands. It is found that the electronic band structure is strongly modified by the apparent nonvanishing ΔE due to the different on-site energies of the MOs of Py and BCSB ligands, and an extra dimerization term, δ, arising from the structural distortion of the $Py(BCSB)_2$. Consequently, the usual highly dispersive Dirac band becomes highly localized driven by the strong electron inhomogeneity, i.e., large ΔE and δ.[4,53] Such strong electron localization further induces spin polarization upon hole doping as observed experimentally,[54] which can be further enhanced by eliminating interlayer interaction and/or increasing the doping concentration.[4,53]

The topological properties of $Py(BCSB)_2$ related to its flat band has been studied,[53] which however requires a large amount of doping to shift to the Fermi level. Soon afterward, another

https://dx.doi.org/10.1021/acs.accounts.0c00652
Acc. Chem. Res. 2021, 54, 416−426

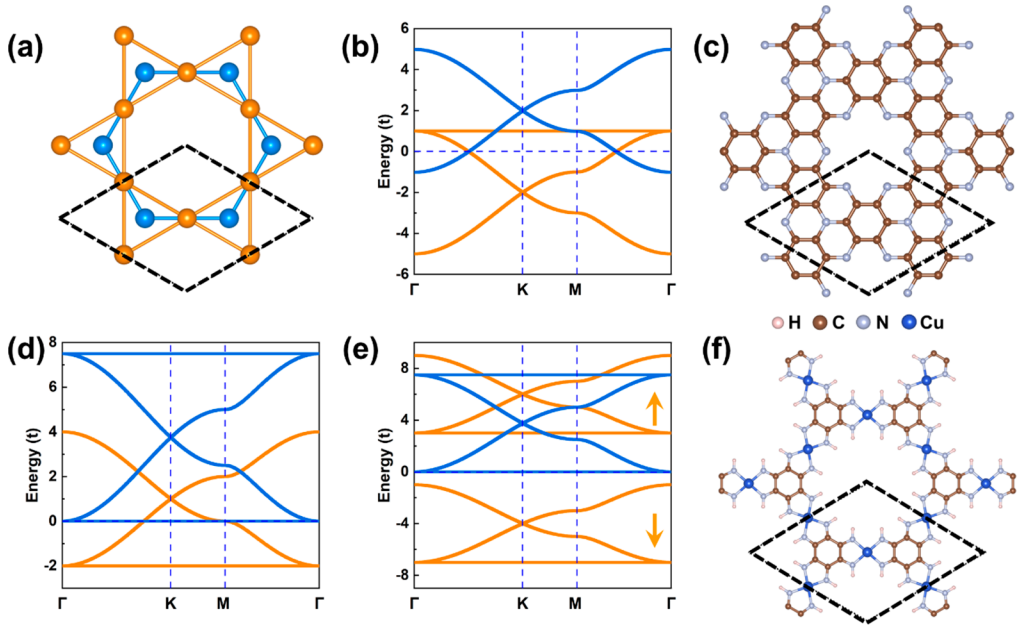

Figure 6. Band structure of the combined honeycomb and Kagome (CHK) lattice. (a) Ball-and-stick model of CHK lattice (blue and orange spheres show honeycomb and Kagome lattice, respectively). (b) Band structure resulting from the overlapping single-orbital H_h and H_k sub-bands, forming a nodal ring at the Fermi level with $\varepsilon_h = 1.985|t|$ and $\varepsilon_k = -|t|$. (c) Representative COF, C_9N_4, where molecular orbitals formed by N and C atoms construct the honeycomb and Kagome lattices, respectively.[56] (d) Band structure with nonmagnetic $p_{x,y}$-orbital honeycomb lattice and single-orbital Kagome lattice with $\varepsilon_h = 3.75t$, $\varepsilon_k = 0$, $pp\sigma = 2.5t$, and $pp\pi = 0$. (e) Same as (d) with strong exchange splitting in the Kagome bands with $M = 5t$. The arrows indicate the spin-up and -down channels. (f) Representative MOF, $Cu_3(HAB)_2$, in which HAB molecules and Cu ions form the honeycomb and Kagome lattices, respectively. The dashed rhombus indicates the unit cell in (c) and (f). The orange and blue bands are the sub-bands of the honeycomb and Kagome lattices, respectively.

family of Lieb lattice materials that host intrinsic topological properties have been demonstrated in phthalocyanine-based MOFs, MPc-MOFs.[55] The crystal structure of MPc-MOFs has the desired Lieb lattice geometry, where the corner- and edge-center sites are occupied by the MPc ligand and the benzene ring, respectively (Figure 5h). The conjugated π electrons of Pc and benzene ligands contribute to the electronic Lieb lattice, while metal ions in the center of MPc provide the spin degree of freedom responsible for their interesting magnetic properties. Due to a large ΔE between Pc and benzene ligands and a strong hybridization (2NN hopping, t_2) between neighboring benzene ligands, the Lieb band structure of MPc-MOFs is also strongly distorted (Figure 4f). Nevertheless, their topological properties that related to the M-point band degeneracy are conserved, and the Fermi level is located right in the gap between the bottom Dirac and middle flat band, rendering MPc-MOFs an intrinsic topological insulator. Through element substitution and/or strain engineering that tunes ΔE to close the gap, topological phase transition among various topological states, e.g., QSH and QAH states, has also been demonstrated.[55]

COMBINED HONEYCOMB AND KAGOME LATTICE

Because of the same unit cell shared by honeycomb and Kagome lattices, and the latter is the line graph of the former, the two can be combined in one lattice (Figure 6a), named combined honeycomb−Kagome (CHK) lattice for convenience. In principle, all the combinations of honeycomb systems in Figure 3 and Kagome systems in Figure 4 could be realized in real material systems. Indeed, such a CHK lattice exists in many MOFs and COFs, where the two sublattices are occupied by different organic ligands and/or metal ions, respectively.[20] When the interaction between the two sublattices is weak, either of the two can be selectively populated around the Fermi level depending on the electron filling. This has been widely observed in various MOFs/COFs, as we demonstrated in the previous sections. There are more complex scenarios when there is a strong coupling between the two sublattices electronically and/or magnetically.

To reveal the exotic bands associated with CHK lattices, one can construct a single-orbital CHK lattice Hamiltonian: $H(\vec{k}) = \begin{pmatrix} H_h & H_{hk} \\ H_{hk}^* & H_k \end{pmatrix}$, where H_h, H_k, and H_{hk} denote the honeycomb, Kagome sublattice Hamiltonian, and their interaction, respectively. For negligible intersublattice interaction ($H_{hk} = 0$), $H(\vec{k})$ is simply block-diagonalized into H_h (eq 3) and H_k (eq 6), leading to two subsets of honeycomb Dirac bands and Kagome bands, respectively. Depending on the on-site energy differences between H_h and H_k, the two subsets of bands may overlap with each other, as shown in Figure 6b. Interestingly, their band crossing points will form a nodal ring around the Γ point, and remain robust for relatively weak H_{hk}. This nodal-ring semimetal state has been found in a carbon nitride COF, C_9N_4, as shown in Figure 6(c).[56] Its nodal ring is located right at the Fermi level, and the two subsets of Dirac and Kagome bands are attributed to MOs formed by N and C atoms on the sub honeycomb and Kagome lattices, respectively. The topological nodal ring is protected by the C_2 rotational symmetry together with the negligible SOC of C and N atoms.

If the subhoneycomb lattice has a (p_x, p_y) orbital basis, H_h takes the form of eq 4 and then the CHK lattice will host either two subsets of four and three bands or seven overlapping bands with a nodal ring, as shown in Figure 6d, depending on the on-site energy difference between H_h and H_k. A more complicated scenario occurs when H_k and H_h represent two different

https://dx.doi.org/10.1021/acs.accounts.0c00652
Acc. Chem. Res. 2021, 54, 416−426

characteristic electrons, e.g., localized d and itinerant π electrons. One example of a band structure with d-electron H_k and π-electron H_h is shown in Figure 6e, where spin-up and -down Kagome bands split, with the spin-degenerate (p_x, p_y) honeycomb bands located in between. Such coexistence of localized spins and conducting electrons is known in many strongly correlated systems, e.g., Kondo and heavy Fermion system,[57,58] which yields a range of intriguing quantum phenomena, such as unconventional superconductivity and giant magnetoresistance (GMR).[59,60]

One prototypical material candidate that hosts the aforementioned hybrid system between localized and diffuse electrons in two sublattices is demonstrated in an experimentally synthesized MOF,[61] Cu-hexaiminobenzene [$Cu_3(HAB)_2$], where HAB ligands and Cu ions form the honeycomb and Kagome lattices, respectively, as shown in Figure 5f. Cu^{2+} ions with d^9 electronic and spin-1/2 configuration prefer antiferromagnetic (AFM) coupling, while the π electrons of HAB in a flat band located around the Fermi level favor a ferromagnetic (FM) state. As such, both d and π electrons are frustrated and, remarkably, coupled through a Hund's type FM coupling, leading to an intriguing competition between local spins and conjugated electrons. This competition may be tuned through either charge doping and/or Coulomb repulsion, which yields a complex quantum phase diagram that spans over quantum spin liquid, Fermi liquid and flat-band ferromagnetic states. These exotic states might be either directly observed through scanning tunneling microscopy measurement or indirectly revealed by GMR measurement via the existence of magnetic polarons.[61]

SUMMARY AND PERSPECTIVES

Beyond the three basic 2D lattices that we have discussed, various exotic topological bands have also been shown in MOFs/COFs with other lattice symmetries, e.g., 2D square and triangle, and 3D molecular crystals.[62−65] Experimental efforts have been inspired to verify the theoretical predictions using different approaches.[66,67] Although some promising MOFs/COFs have been synthesized and analyzed experimentally,[46,50,54,68] the definite and unambiguous evidence of topological character, such as nontrivial topological edge state and quantized edge conductivity, has yet to be confirmed, likely due to small crystalline sample size, low sample quality, and/or negative substrate influence.[66,67] On the other hand, if confirmed, MOFs and COFs have some distinct advantages over inorganic counterparts, e.g., long spin coherence time and high tunability in both structural symmetry and charge doping, which may reveal new physical phenomena and facilitate their applications in organic electronics and spintronics.[69,70] Efforts in growing large-area and high-quality MOFs/COFs, including on weakly interacting substrate, are widely ongoing. Also, other lines of active experimental efforts have been devoted to investigating strongly correlated quantum states in MOFs/COFs, such as superconductivity,[71,72] frustrated quantum spin liquid,[73] and two-level quantum information systems,[74,75] where notable progress has been made. We note that the study of exotic band structures and intriguing quantum states in MOFs/COFs is still at its infancy and much more remains to be explored. We envision a rapid growth of this emerging field in the near future with ample excitement awaiting ahead.

AUTHOR INFORMATION

Corresponding Author

Feng Liu − *Department of Materials Science and Engineering, University of Utah, Salt Lake City, Utah 84112, United States;* orcid.org/0000-0002-3701-8058; Email: fliu@eng.utah.edu

Authors

Wei Jiang − *Department of Electrical and Computer Engineering, University of Minnesota, Minneapolis, Minnesota 55455, United States;* orcid.org/0000-0001-6167-1156

Xiaojuan Ni − *Department of Materials Science and Engineering, University of Utah, Salt Lake City, Utah 84112, United States;* orcid.org/0000-0002-5845-7404

Complete contact information is available at: https://pubs.acs.org/10.1021/acs.accounts.0c00652

Author Contributions

§W.J. and X.N. contributed equally. The manuscript was written through contributions of all authors. All authors have given approval to the final version of the manuscript.

Notes

The authors declare no competing financial interest.

Biographies

Wei Jiang is a Postdoctoral Fellow at the University of Minnesota. He received his Ph.D. in Materials Science and Engineering from the University of Utah in 2018. His main research interests are exotic electronic and magnetic states in MOFs/COFs; topological materials for electronic and spintronics applications.

Xiaojuan Ni is a Postdoctoral Fellow at the University of Arizona. She received her Ph.D. in Materials Science and Engineering from the University of Utah in 2020. Her main research interests are electronic, magnetic, and topological properties of MOFs/COFs.

Feng Liu is a Professor of Materials Science and Engineering and an adjunct professor of Physics at the University of Utah, a Fellow of the American Physical Society. He received his Ph.D. in Chemical Physics from Virginia Commonwealth University in 1990. His research interests lie in theoretical modeling and computational simulation, from the atomic to continuum scale, of properties of surface/interface and thin-film materials, with a recent focus on 2D topological materials, in particular organic topological materials reviewed in this Account.

ACKNOWLEDGMENTS

This work is supported by U.S. Department of Energy-Basic Energy Sciences (Grant No. DE-FG02-04ER46148).

REFERENCES

(1) Wang, Z. F.; Liu, Z.; Liu, F. Organic Topological Insulators in Organometallic Lattices. *Nat. Commun.* **2013**, *4*, 1471.

(2) Liu, Z.; Wang, Z. F.; Mei, J. W.; Wu, Y. S.; Liu, F. Flat Chern Band in a Two-Dimensional Organometallic Framework. *Phys. Rev. Lett.* **2013**, *110*, 106804.

(3) Wang, Z. F.; Su, N.; Liu, F. Prediction of a Two-Dimensional Organic Topological Insulator. *Nano Lett.* **2013**, *13*, 2842−2845.

(4) Jiang, W.; Huang, H.; Liu, F. A Lieb-like Lattice in a Covalent-Organic Framework and Its Stoner Ferromagnetism. *Nat. Commun.* **2019**, *10*, 2207.

(5) Novoselov, K. S.; Geim, A. K.; Morozov, S. V.; Jiang, D.; Katsnelson, M. I.; Grigorieva, I. V.; Dubonos, S. V.; Firsov, A. A. Two-

Dimensional Gas of Massless Dirac Fermions in Graphene. *Nature* **2005**, *438*, 197−200.
(6) Wallace, P. R. The Band Theory of Graphite. *Phys. Rev.* **1947**, *71*, 622−634.
(7) Liu, Z.; Liu, F.; Wu, Y. S. Exotic Electronic States in the World of Flat Bands: From Theory to Material. *Chin. Phys. B* **2014**, *23*, 077308.
(8) Tasaki, H. Ferromagnetism in the Hubbard Models with Degenerate Single-Electron Ground States. *Phys. Rev. Lett.* **1992**, *69*, 1608−1611.
(9) Mielke, A. Exact Ground States for the Hubbard Model on the Kagome Lattice. *J. Phys. A: Math. Gen.* **1992**, *25*, 4335−4345.
(10) Mukherjee, S.; Spracklen, A.; Choudhury, D.; Goldman, N.; Öhberg, P.; Andersson, E.; Thomson, R. R. Observation of a Localized Flat-Band State in a Photonic Lieb Lattice. *Phys. Rev. Lett.* **2015**, *114*, 245504.
(11) Zong, Y.; Xia, S.; Tang, L.; Song, D.; Hu, Y.; Pei, Y.; Su, J.; Li, Y.; Chen, Z. Observation of Localized Flat-Band States in Kagome Photonic Lattices. *Opt. Express* **2016**, *24*, 8877−8885.
(12) The physical origins and properties of flat and Dirac bands are distinct. Dirac bands result from symmetry protected band crossing points characterized with linear band dispersion (zero effective mass). The slope of Dirac bands is proportional to the magnitude of lattice hopping parameters, independent of how small a slope (i.e., how flat) the bands are. In contrast, topological flat bands result from phase cancellation of lattice wave functions (i.e., destructive quantum interference), characterized with localized plaquette states in real space. The topological flat bands remain in principle perfectly flat (nondispersive with infinite effective mass), independent of the magnitude of lattice hopping; they will only develop finite dispersion when additional interaction, such as spin−orbit interaction, is considered.
(13) Chiu, C.-K.; Teo, J. C. Y.; Schnyder, A. P.; Ryu, S. Classification of Topological Quantum Matter with Symmetries. *Rev. Mod. Phys.* **2016**, *88*, 35005.
(14) Huang, H.; Liu, F. others. A Unified View of Topological Phase Transition in Band Theory. *Research* **2020**, *2020*, 7832610.
(15) Berry, M. V. Quantal Phase Factors Accompanying Adiabatic Changes. *Proc. R. Soc. London. A. Math. Phys. Sci.* **1984**, *392*, 45−57.
(16) Klitzing, K. v.; Dorda, G.; Pepper, M. New Method for High-Accuracy Determination of the Fine-Structure Constant Based on Quantized Hall Resistance. *Phys. Rev. Lett.* **1980**, *45*, 494−497.
(17) Kane, C. L.; Mele, E. J. Quantum Spin Hall Effect in Graphene. *Phys. Rev. Lett.* **2005**, *95*, 226801.
(18) Bernevig, B. A.; Hughes, T. L.; Zhang, S.-C. Quantum Spin Hall Effect and Topological Phase Transition in HgTe Quantum Wells. *Science (Washington, DC, U. S.)* **2006**, *314*, 1757−1761.
(19) Wang, Z. F.; Jin, K.; Liu, F. Computational Design of Two-Dimensional Topological Materials. *WIREs Comput. Mol. Sci.* **2017**, *7*, No. e1304.
(20) Jiang, W.; Liu, F. Organic Topological Insulators. In *World Scientific Reference on Spin in Organics*; Materials and Energy; World Scientific, 2017; pp 201−224.
(21) Springer, M. A.; Liu, T. J.; Kuc, A.; Heine, T. Topological Two-Dimensional Polymers. *Chem. Soc. Rev.* **2020**, *49*, 2007−2019.
(22) Hasan, M. Z.; Kane, C. L. Colloquium: Topological Insulators. *Rev. Mod. Phys.* **2010**, *82*, 3045−3067.
(23) Qi, X.-L.; Zhang, S.-C. Topological Insulators and Superconductors. *Rev. Mod. Phys.* **2011**, *83*, 1057−1110.
(24) Feng, X.; Ding, X.; Jiang, D. Covalent Organic Frameworks. *Chem. Soc. Rev.* **2012**, *41*, 6010−6022.
(25) Zhou, H. C. J.; Kitagawa, S. Metal-Organic Frameworks (MOFs). *Chem. Soc. Rev.* **2014**, *43*, 5415−5418.
(26) Haldane, F. D. M. Model for a Quantum Hall Effect without Landau Levels: Condensed-Matter Realization of the "Parity Anomaly. *Phys. Rev. Lett.* **1988**, *61*, 2015−2018.
(27) Slater, J. C.; Koster, G. F. Simplified LCAO Method for the Periodic Potential Problem. *Phys. Rev.* **1954**, *94*, 1498−1524.
(28) Kane, C. L.; Mele, E. J. Z2 Topological Order and the Quantum Spin Hall Effect. *Phys. Rev. Lett.* **2005**, *95*, 146802.
(29) Fu, L.; Kane, C. L. Topological Insulators with Inversion Symmetry. *Phys. Rev. B: Condens. Matter Mater. Phys.* **2007**, *76*, 045302.
(30) Thouless, D. J.; Kohmoto, M.; Nightingale, M. P.; den Nijs, M. Quantized Hall Conductance in a Two-Dimensional Periodic Potential. *Phys. Rev. Lett.* **1982**, *49*, 405−408.
(31) Su, N.; Jiang, W.; Wang, Z.; Liu, F. Prediction of Large Gap Flat Chern Band in a Two-Dimensional Metal-Organic Framework. *Appl. Phys. Lett.* **2018**, *112*, 033301.
(32) Wang, Z. F.; Liu, Z.; Liu, F. Quantum Anomalous Hall Effect in 2D Organic Topological Insulators. *Phys. Rev. Lett.* **2013**, *110*, 196801.
(33) Hu, H.; Wang, Z.; Liu, F. Half Metal in Two-Dimensional Hexagonal Organometallic Framework. *Nanoscale Res. Lett.* **2014**, *9*, 690.
(34) Kim, H. J.; Li, C.; Feng, J.; Cho, J. H.; Zhang, Z. Competing Magnetic Orderings and Tunable Topological States in Two-Dimensional Hexagonal Organometallic Lattices. *Phys. Rev. B: Condens. Matter Mater. Phys.* **2016**, *93*, No. 041404(R).
(35) Pavliček, N.; Mistry, A.; Majzik, Z.; Moll, N.; Meyer, G.; Fox, D. J.; Gross, L. Synthesis and Characterization of Triangulene. *Nat. Nanotechnol.* **2017**, *12*, 308−311.
(36) Galeotti, G.; De Marchi, F.; Hamzehpoor, E.; MacLean, O.; Rajeswara Rao, M.; Chen, Y.; Besteiro, L. V.; Dettmann, D.; Ferrari, L.; Frezza, F.; Sheverdyaeva, P. M.; Liu, R.; Kundu, A. K.; Moras, P.; Ebrahimi, M.; Gallagher, M. C.; Rosei, F.; Perepichka, D. F.; Contini, G. Synthesis of Mesoscale Ordered Two-Dimensional π-Conjugated Polymers with Semiconducting Properties. *Nat. Mater.* **2020**, *19*, 874−880.
(37) Jing, Y.; Heine, T. Making 2D Topological Polymers a Reality. *Nat. Mater.* **2020**, *19*, 823−824.
(38) Jing, Y.; Heine, T. Two-Dimensional Kagome Lattices Made of Hetero Triangulenes Are Dirac Semimetals or Single-Band Semiconductors. *J. Am. Chem. Soc.* **2019**, *141*, 743−747.
(39) Zhou, M.; Ming, W.; Liu, Z.; Wang, Z.; Li, P.; Liu, F. Epitaxial Growth of Large-Gap Quantum Spin Hall Insulator on Semiconductor Surface. *Proc. Natl. Acad. Sci. U. S. A.* **2014**, *111*, 14378−14381.
(40) Zhou, M.; Ming, W.; Liu, Z.; Wang, Z.; Yao, Y.; Liu, F. Formation of Quantum Spin Hall State on Si Surface and Energy Gap Scaling with Strength of Spin Orbit Coupling. *Sci. Rep.* **2015**, *4*, 7102.
(41) Ni, X.; Huang, H.; Liu, F. Robustness of Topological Insulating Phase against Vacancy, Vacancy Cluster, and Grain Boundary Bulk Defects. *Phys. Rev. B: Condens. Matter Mater. Phys.* **2020**, *101*, 125114.
(42) Zhou, Y.; Sethi, G.; Liu, H.; Liu, F. Excited Quantum Hall Effect: Enantiomorphic Flat Bands in a Yin-Yang Kagome Lattice. *arXiv (Materials Science)*, October 16, 2019, 1908.03689, ver. 2. https://arxiv.org/abs/1908.03689.
(43) Zhou, Y.; Sethi, G.; Zhang, C.; Ni, X.; Liu, F. Giant Intrinsic Circular Dichroism of Enantiomorphic Flat Chern Bands and Flatband Devices. *Phys. Rev. B: Condens. Matter Mater. Phys.* **2020**, *102*, 125115.
(44) Gao, Y.; Zhang, Y.-Y.; Sun, J.-T.; Zhang, L.; Zhang, S.; Du, S. Quantum Anomalous Hall Effect in Two-Dimensional Cu-Dicyanobenzene Coloring-Triangle Lattice. *Nano Res.* **2020**, *13*, 1571−1575.
(45) Ni, X.; Zhou, Y.; Sethi, G.; Liu, F. π-Orbital Yin-Yang Kagome Bands in Anilato-Based Metal-Organic Frameworks. *Phys. Chem. Chem. Phys.* **2020**, *22*, 25827−25832.
(46) Kambe, T.; Sakamoto, R.; Kusamoto, T.; Pal, T.; Fukui, N.; Hoshiko, K.; Shimojima, T.; Wang, Z.; Hirahara, T.; Ishizaka, K.; Hasegawa, S.; Liu, F.; Nishihara, H. Redox Control and High Conductivity of Nickel Bis(Dithiolene) Complex π-Nanosheet: A Potential Organic Two-Dimensional Topological Insulator. *J. Am. Chem. Soc.* **2014**, *136*, 14357−14360.
(47) Zhang, L. Z.; Wang, Z. F.; Huang, B.; Cui, B.; Wang, Z.; Du, S. X.; Gao, H. J.; Liu, F. Intrinsic Two-Dimensional Organic Topological Insulators in Metal-Dicyanoanthracene Lattices. *Nano Lett.* **2016**, *16*, 2072−2075.
(48) Zhang, X.; Wang, Z.; Zhao, M.; Liu, F.; Gr, P. Tunable Topological States in Electron-Doped HTT-Pt. *Phys. Rev. B: Condens. Matter Mater. Phys.* **2016**, *93*, 165401.

https://dx.doi.org/10.1021/acs.accounts.0c00652
Acc. Chem. Res. 2021, 54, 416−426

(49) Ni, X.; Jiang, W.; Huang, H.; Jin, K. H.; Liu, F. Intrinsic Quantum Anomalous Hall Effect in a Two-Dimensional Anilato-Based Lattice. *Nanoscale* **2018**, *10*, 11901−11906.
(50) Chisnell, R.; Helton, J. S.; Freedman, D. E.; Singh, D. K.; Bewley, R. I.; Nocera, D. G.; Lee, Y. S. Topological Magnon Bands in a Kagome Lattice Ferromagnet. *Phys. Rev. Lett.* **2015**, *115*, 147201.
(51) Zhang, S.; Kang, M.; Huang, H.; Jiang, W.; Ni, X.; Kang, L.; Zhang, S.; Xu, H.; Liu, Z.; Liu, F. Kagome Bands Disguised in a Coloring-Triangle Lattice. *Phys. Rev. B: Condens. Matter Mater. Phys.* **2019**, *99*, No. 100404(R).
(52) Jiang, W.; Kang, M.; Huang, H.; Xu, H.; Low, T.; Liu, F. Topological Band Evolution between Lieb and Kagome Lattices. *Phys. Rev. B: Condens. Matter Mater. Phys.* **2019**, *99*, 125131.
(53) Cui, B.; Zheng, X.; Wang, J.; Liu, D.; Xie, S.; Huang, B. Realization of Lieb Lattice in Covalent-Organic Frameworks with Tunable Topology and Magnetism. *Nat. Commun.* **2020**, *11*, 66.
(54) Jin, E.; Asada, M.; Xu, Q.; Dalapati, S.; Addicoat, M. A.; Brady, M. A.; Xu, H.; Nakamura, T.; Heine, T.; Chen, Q.; Jiang, D. Two-Dimensional Sp2 Carbon-Conjugated Covalent Organic Frameworks. *Science (Washington, DC, U. S.)* **2017**, *357*, 673−676.
(55) Jiang, W.; Zhang, S.; Wang, Z.; Liu, F.; Low, T. Topological Band Engineering of Lieb Lattice in Phthalocyanine-Based Metal-Organic Frameworks. *Nano Lett.* **2020**, *20*, 1959−1966.
(56) Chen, H.; Zhang, S.; Jiang, W.; Zhang, C.; Guo, H.; Liu, Z.; Wang, Z.; Liu, F.; Niu, X. Prediction of Two-Dimensional Nodal-Line Semimetals in a Carbon Nitride Covalent Network. *J. Mater. Chem. A* **2018**, *6*, 11252−11259.
(57) Anderson, P. W. Localized Magnetic States in Metals. *Phys. Rev.* **1961**, *124*, 41−53.
(58) Kondo, J. Resistance Minimum in Dilute Magnetic Alloys. *Prog. Theor. Phys.* **1964**, *32*, 37−49.
(59) Oliveira, N. F.; Foner, S.; Shapira, Y.; Reed, T. B. EuTe. I. Magnetic Behavior of Insulating and Conducting Single Crystals. *Phys. Rev. B* **1972**, *5*, 2634−2646.
(60) Lee, P. A.; Nagaosa, N.; Wen, X.-G. Doping a Mott Insulator: Physics of High-Temperature Superconductivity. *Rev. Mod. Phys.* **2006**, *78*, 17−85.
(61) Jiang, W.; Liu, Z.; Mei, J. W.; Cui, B.; Liu, F. Dichotomy between Frustrated Local Spins and Conjugated Electrons in a Two-Dimensional Metal-Organic Framework. *Nanoscale* **2019**, *11*, 955−961.
(62) Zhang, L. Z.; Wang, Z. F.; Wang, Z. M.; Du, S. X.; Gao, H. J.; Liu, F. Highly Anisotropic Dirac Fermions in Square Graphynes. *J. Phys. Chem. Lett.* **2015**, *6*, 2959−2962.
(63) Liu, Z.; Mei, J. W.; Liu, F. First-Principles Study of the Organometallic S = 1/2 Kagome Compound Cu(1,3-Bdc). *Phys. Rev. B: Condens. Matter Mater. Phys.* **2015**, *92*, 165101.
(64) Liu, Z.; Wang, H.; Wang, Z. F.; Yang, J.; Liu, F. Pressure-Induced Organic Topological Nodal-Line Semimetal in the Three-Dimensional Molecular Crystal Pd(Dddt)2. *Phys. Rev. B: Condens. Matter Mater. Phys.* **2018**, *97*, 155138.
(65) Wang, A.; Zhao, X.; Zhao, M.; Zhang, X.; Feng, Y.; Liu, F. Kane Fermion in a Two-Dimensional π-Conjugated Bis(Iminothiolato)-Nickel Monolayer. *J. Phys. Chem. Lett.* **2018**, *9*, 614−619.
(66) Gao, Z.; Hsu, C. H.; Liu, J.; Chuang, F. C.; Zhang, R.; Xia, B.; Xu, H.; Huang, L.; Jin, Q.; Liu, P. N.; Lin, N. Synthesis and Characterization of a Single-Layer Conjugated Metal-Organic Structure Featuring a Non-Trivial Topological Gap. *Nanoscale* **2019**, *11*, 878−881.
(67) Kumar, A.; Banerjee, K.; Foster, A. S.; Liljeroth, P. Two-Dimensional Band Structure in Honeycomb Metal-Organic Frameworks. *Nano Lett.* **2018**, *18*, 5596−5602.
(68) Sun, X.; Wu, K.-H.; Sakamoto, R.; Kusamoto, T.; Maeda, H.; Ni, X.; Jiang, W.; Liu, F.; Sasaki, S.; Masunagae, H.; Nishihara, H. Bis(Aminothiolato)Nickel Nanosheet as a Redox Switch for Conductivity and an Electrocatalyst for the Hydrogen Evolution Reaction. *Chem. Sci.* **2017**, *8*, 8078−8085.
(69) Kelley, T. W.; Baude, P. F.; Gerlach, C.; Ender, D. E.; Muyres, D.; Haase, M. A.; Vogel, D. E.; Theiss, S. D. Recent Progress in Organic Electronics: Materials, Devices, and Processes. *Chem. Mater.* **2004**, *16*, 4413−4422.
(70) Naber, W. J. M.; Faez, S.; Wiel, W. G. van der. Organic Spintronics. *J. Phys. D: Appl. Phys.* **2007**, *40*, R205−R228.
(71) Zhang, X.; Zhou, Y.; Cui, B.; Zhao, M.; Liu, F. Theoretical Discovery of a Superconducting Two-Dimensional Metal–Organic Framework. *Nano Lett.* **2017**, *17*, 6166−6170.
(72) Huang, X.; Zhang, S.; Liu, L.; Yu, L.; Chen, G.; Xu, W.; Zhu, D. Superconductivity in a Copper(II)-Based Coordination Polymer with Perfect Kagome Structure. *Angew. Chem., Int. Ed.* **2018**, *57*, 146−150.
(73) Misumi, Y.; Yamaguchi, A.; Zhang, Z.; Matsushita, T.; Wada, N.; Tsuchiizu, M.; Awaga, K. Quantum Spin Liquid State in a Two-Dimensional Semiconductive Metal-Organic Framework. *J. Am. Chem. Soc.* **2020**, *142*, 16513−16517.
(74) Clemente-Juan, J. M.; Coronado, E.; Gaita-Ariño, A. Magnetic Polyoxometalates: From Molecular Magnetism to Molecular Spintronics and Quantum Computing. *Chem. Soc. Rev.* **2012**, *41*, 7464−7478.
(75) Aromí, G.; Aguilà, D.; Gamez, P.; Luis, F.; Roubeau, O. Design of Magnetic Coordination Complexes for Quantum Computing. *Chem. Soc. Rev.* **2012**, *41*, 537−546.

https://dx.doi.org/10.1021/acs.accounts.0c00652
Acc. Chem. Res. 2021, 54, 416−426